Evaluation of QED backgrounds for an e^+e^- linear collider in deep quantum beamstrahlung regime

T. Ohgaki and M. Xie
Lawrence Berkeley National Laboratory, Berkeley, California 94720
(May 1999)

We investigate the QED backgrounds induced by the beam-beam interaction in a 5 TeV e^+e^- linear collider, especially in the deep quantum regime (Beamstrahlung parameter $\Upsilon \gg 1$). Beamstrahlung during the collision of the e^+e^- linear colliders in the deep quantum regime is expected to lose larger energy of the beams and to create much larger number of the electron-positron pairs, than in the classical and intermediate regimes ($\Upsilon \lesssim 1$). In order to reduce the effects, we take an approach, based on an effect known as quantum suppression of beamstrahlung. For the design of linear colliders, the electron-positron pair production from real and virtual photons in the arbitrary Υ regime is derived. For particle physics experiment, the e^+e^-, $e\gamma$ and $\gamma\gamma$ luminosity distribution in a 5 TeV e^+e^- linear collider are discussed with simulation.

I. INTRODUCTION

One of the most important constraint on the performance of an e^+e^- linear collider is beamstrahlung [1–3] due to the beam-beam interaction [3]. Beamstrahlung is the synchrotron radiation produced by electrons and positrons as they pass through the collective electromagnetic field of the oncoming beam. The fields can be so strong due to the extremely high charge density that colliding particles may lose significant amount of their energy, causing severe luminosity degradation. The beamstrahlung photons may also turn to copious e^+e^- pairs and the pairs are strongly deflected as they continue moving through the collective field, causing troublesome background problem to the study of particle physics.

Beamstrahlung can be classified into three regimes [3] according to the magnitude of the beamstrahlung parameter, $\Upsilon = \gamma B/B_c$, where $\gamma = E/m$, E is the beam energy, B the beam field, and B_c the Schwinger critical field. The three regimes are, respectively, the classical regime if $\Upsilon \ll 1$, the extreme or deep quantum regime if $\Upsilon \gg 1$, and in between the intermediate regime. In the classical regime, beamstrahlung can be calculated with the usual synchrotron radiation formula derived from classical electrodynamics. Alternatively, the beamstrahlung parameter may be expressed as $\Upsilon = 2\omega_c/3E$ in terms of a classical quantity known as critical photon energy ω_c. The classical theory is valid only if the energy of the radiated photon, characterized by ω_c, is much less than the kinetic energy of the radiating particle. This condition corresponds to $\Upsilon \ll 1$.

So far, all the designs of linear colliders at 0.5 TeV have managed to stay in the regime with $\Upsilon < 1$ [4], where beamstrahlung and its deleterious effects can be reduced by having smaller Υ. Therefore reducing Υ by reducing the beam field, has been adopted as a guideline and that is made possible by taking the flat beam approach. However, as we know the required luminosity for a collider has to rise as the square of its center-of-mass energy, thus to keep wall plug power under control the beam has to be focused to smaller size with higher charge density, this will unavoidably raise Υ and put a linear collider into the deep quantum regime. As a result, the flat beam approach will become more difficult and less effective at higher energy. More difficult for technical reason, as it requires the beam size in one transverse direction to be much smaller (for given beam area), thus pushing the limit for tight beam positioning control at higher energy. For current designs at 0.5 TeV, the vertical beam size is already down to a few nanometers. The flat beam approach is less effective for physical reason, as it has been shown the dependence of the spread in luminosity spectrum on beam shape becomes very weak in the deep quantum regime [5].

As Υ increases due to either stronger fields or higher energy of the beam, the radiated photons become more energetic. Quantum theory has to be used to take into account radiation recoil and the fact that photon spectrum beyond the particle energy is kinetically forbidden. A full quantum treatment of synchrotron radiation was given by Sokolov *et al.* for arbitrary value of Υ in a constant field [6]. This result was later applied to and extended for the study of beamstrahlung [1–3,5,7].

According to the quantum theory, beamstrahlung scales differently in the regimes $\Upsilon \ll 1$ and $\Upsilon \gg 1$. It was shown that advantage may be taken of this behavior in the deep quantum regime to extend collider energy to multi-TeV without excessive beamstrahlung [2]. It was also made clear that the beam parameters required to take advantage of this effect, such as very short bunch or small emittance, are not readily achievable, and the flat beam approach is a much better choice at 0.5 TeV energy range.

However, one should not forget that 0.5 TeV energy is only a near term goal for linear collider development, very much limited by the current technologies. Considering competitions from hadron or even muon colliders, it would be much more compelling for linear collider to go beyond that energy. During a recent Snowmass Workshop on New Directions for High-Energy Physics in 1996 [8] and later on in the 7th and 8th Workshops on Advanced Accelerator Concepts [9], accelerator community has made an interesting attempt to consider various accelerator issues and interaction point (IP) approaches at an energy of 5 TeV.

In particular, the possibility of employing quantum suppression as an IP approach was explored over a wide range of beam parameters at 5 TeV by Xie *et al* [10]. It was shown in this study that when the major accelerator and IP constraints are taken into account, it becomes increasingly necessary to operate linear colliders in high Υ regime and use the quantum effect to suppress beamstrahlung to our advantage.

In this paper, we discuss an effect known as quantum suppression of beamstrahlung (QSB) [10]. The very high energy collider designs, for example, the laser driven e^+e^- linear colliders [10], can be accessible to be in the deep quantum regime $\Upsilon \gg 1$, because of the very short bunch lengths. Full blown Monte-Carlo simulation was performed to study luminosity spectrum under the influence of all major electromagnetic (EM) and quantum electrodynamics (QED) processes at the IP, including disruption, beamstrahlung, coherent and incoherent pair creations. In Sec. II, we estimate the classical effects by the beam-beam interaction at a 5 TeV e^+e^- linear collider. In Sec. III, we investigate the quantum effects by the beam-beam interaction at 5 TeV energy and we drive the coherent and incoherent pair creation in arbitrary Υ regime. In Sec. IV, we discuss about the $e^+e^-, e\gamma$ and $\gamma\gamma$ luminosity distribution in a 5 TeV e^+e^- linear collider with simulation.

II. CLASSICAL PHENOMENA

A. Luminosity enhancement

The beam-beam interaction can be classified into the classical and quantum phenomena. The classical effects are mainly the enhancement of the luminosity due to the electromagnetic attraction and the deflection of the individual particles. In this section, we estimate the classical effects of the beam-beam interaction at a 5 TeV e^+e^- linear collider.

Due to the attractive Coulomb force between the electron and positron beams, the beams pinch into each other and they are deflected during beam-beam collision. The deformation of the colliding beams results in the enhancement of the luminosity. The disruption parameter, which is defined as the ratio of the rms bunch length σ_z to the focal length, is [3]

$$D_{x(y)} \equiv \frac{2Nr_e}{\gamma}\frac{\sigma_z}{\sigma_{x(y)}(\sigma_x+\sigma_y)}, \tag{1}$$

where N is the number of the initial particles per bunch, r_e the classical electron radius, γ the Lorentz factor of the beams, and σ_x, σ_y the rms transverse sizes of beams at the IP. The number of oscillations of particles within the oncoming beam is given by $n = \sqrt{\sqrt{3}D}/2\pi$ [3], when we assume a uniform longitudinal distribution of the bunch for simplicity. The depth-of-focus parameter is [3]

$$A_{x(y)} \equiv \frac{\sigma_z}{\beta^*_{x(y)}}, \tag{2}$$

where β^* is the β-function at the IP. The beam parameters of an e^+e^- linear collider with the laser drive at $\sqrt{s}_{e^+e^-} = 5$ TeV are listed in Table I [10]. For the chosen parameters, we find $D_x = D_y = 0.29$, $A_x = A_y = 1.6 \times 10^{-2}$, and $n_x = n_y = 0.11$. The beam-beam parameters given by the formulas are listed in Table II. Owing to the very short bunch length σ_z in the chosen parameters, the depth-of-focus parameters are small and the final angle of the initial particles after collision is mainly dominated by the disruption effect. In order to reduce the energy loss of electrons and positrons by beamstrahlung, the very flat beams $\sigma_x \gg \sigma_y$ at the IP are assumed in the next-generation linear colliders (NLC) which are not a kind of the laser driven e^+e^- linear collider, because the strength of the magnetic field of flat beams is smaller than that of round beams. The transverse beam sizes of our case are assumed as round beams, because it has been shown the dependence of the spread in luminosity spectrum on the beam shape becomes very weak in the deep quantum regime [5]. Therefore the oscillations of the particles to the vertical direction at the NLC are larger than those of our case.

The nominal luminosity for head-on collision of Gaussian beams without the disruption effect is

$$L_{00} = f_c\frac{N^2}{4\pi\sigma_x\sigma_y}, \tag{3}$$

where f_c is the repetition rate. For the above beam parameters, we find $L_{00} = 1.0 \times 10^{35}\text{cm}^{-2}\text{s}^{-1}$. The geometrical luminosity with taking into account the variation of the beam cross section due to the change of the β-function around the IP is

$$L_0 = \eta_A L_{00}, \tag{4}$$

where the geometrical factor η_A is [11]

$$\eta_A = \frac{2}{\sqrt{\pi}\sigma_z} \int_0^\infty \frac{e^{-z^2/\sigma_z^2}}{1 + z^2/\beta^{*2}} dz. \tag{5}$$

Since the parameters $A_{x(y)} \ll 1$ in this case, $\eta_A \simeq 1$ results in $L_0 \simeq L_{00}$.

When the disruption is included, the effective luminosity L would be different from L_0. The luminosity enhancement factor is defined as

$$H_D = L/L_0. \tag{6}$$

In the case of $D_x < O(1)$ for the round Gaussian beams, we can use the following formula of the luminosity enhancement factor [3]

$$H_D = 1 + 2D_x/(3\sqrt{\pi}). \tag{7}$$

We find $H_D = 1.1$ and the effective luminosity $L = 1.1 \times 10^{35}\text{cm}^{-2}\text{s}^{-1}$ for above parameters in this study.

Evidently, the procedure does not consider the effects of beamstrahlung and the emission of hard photons in $\Upsilon \gg 1$ is relatively larger than that in $\Upsilon \lesssim 1$, thus we need to rely on the simulation including both the classical and quantum effects of the beam-beam interaction. Here we present the full-blown IP simulation using CAIN developed by Yokoya *et al* [12]. CAIN is capable of handling all major EM and QED processes occurred at the IP, including disruption, beamstrahlung, coherent and incoherent pair creation. It is a Monte-Carlo code which follows beam particles, photons, and pairs in six-dimensional phase space, as well as their spins and polarization. In comparison, the previous studies of beamstrahlung in the deep quantum regime were concentrated mainly on obtaining analytical and semi-analytical results to understand the physics, thus were limited to treating only simple, idealistic models [1,2,5,7]. In these early studies, either disruption, multiple beamstrahlung, or both were neglected, and none was able to treat simultaneously the pair production and give angular-momentum distributions. However this information is essential to background analysis at the interaction region (IR) and the overall assessment of collider performance, especially in high Υ regime. We will discuss about the luminosity distribution at a 5 TeV e^+e^- linear collider with simulation in Sec.IV.

B. Disruption angle

The deflection angle which is the outgoing angle of the full energy particles is characterized by the disruption angle [3]

$$\theta_0 \equiv \frac{2Nr_e}{\gamma(\sigma_x + \sigma_y)} = \frac{D_x\sigma_x}{\sigma_z} = \frac{D_y\sigma_y}{\sigma_z}. \tag{8}$$

The rms angles are $\theta_{x,\text{rms}} = \theta_{y,\text{rms}} = 0.550\theta_0$ and the rms total angle $\theta_{\text{rms}} = \sqrt{2}\theta_{x,\text{rms}}$ in the case of the round beams. For the chosen parameters, we find $\theta_0 = 0.16$ mrad and $\theta_{\text{rms}} = 0.13$ mrad.

In future e^+e^- linear colliders, we need to expect the charged particles with energies much lower than the initial beam energy due to processes such as beamstrahlung and pair creation. Here we consider a particle with $\epsilon E_0 (\epsilon \ll 1)$ where E_0 is the energy of the initial beam. The effective disruption parameters D_x/ϵ and D_y/ϵ can be very large so that the outgoing angle is much larger than that of the full energy particles. The pair creation process generates simultaneously same and opposite charged particles and the trajectories of the opposite charged particles in the oncoming beam are different from those of the same charged particles.

Same charge particles are focused by the oncoming beam and oscillate within the beam. The number of oscillations of particles with ϵE_0 is given by $n = \sqrt{\sqrt{3}D/\epsilon}/2\pi$ [3] and the lower energy particles oscillate more frequently. The maximum deflection angle of the same charge particles near the center of the beams for the x and y dimensions is [3]

$$\theta_{x(y),max} \sim \begin{cases} \theta_0/\epsilon & (D_{x(y)}/\epsilon \lesssim 1/\sqrt{3}) \\ \theta_0/\sqrt{\sqrt{3}\epsilon D_{x(y)}} & (D_{x(y)}/\epsilon \gtrsim 1/\sqrt{3}). \end{cases} \tag{9}$$

When D/ϵ is large, opposite charge particles frequently oscillate and are deflected out of the beam. The maximum deflection angle of the opposite charge particles for the x and y dimensions is [3]

$$\theta_{x(y),max} \sim \begin{cases} \theta_0/\epsilon & (D_{x(y)}/\epsilon \lesssim 1) \\ \left[\ln(4\sqrt{3}D_{x(y)}/\epsilon)/(\sqrt{3}\epsilon D_{x(y)})\right]^{1/2}\theta_0 & (D_{x(y)}/\epsilon \gtrsim 1). \end{cases} \tag{10}$$

Here the maximum angle $\theta_{max} = \sqrt{2}\theta_{x(y),max}$ in the case of the round beams. These maximum deflection angles are compared with the simulation results of the pair creation in the next section.

III. QUANTUM PHENOMENA

A. Sokolov-Ternov formula

The magnetic field in the bunch during collision is of the order of mega-Teslas in the deep quantum regime. Thus, the synchrotron radiation which is called beamstrahlung plays an important role when the electron or positron beam is going through another bunch. The Upsilon parameter, which is described as the ratio of the strength of the magnetic field B (which means $|B|+|E|$) in the bunch to that of the critical magnetic field B_c defined as $B_c = m^2/e \approx 4.4$ GTeslas, is [3]

$$\Upsilon = \frac{2}{3}\frac{\omega_c}{E} = \frac{\lambda\!\!\!^{-}_e\gamma^2}{\rho} = \gamma\frac{B}{B_c} = \frac{e}{m^3}\sqrt{|(F_{\mu\nu}p^\nu)^2|}, \tag{11}$$

where $\lambda\!\!\!^{-}_e$ is the Compton wavelength, ρ the orbit radius of curvature, $F_{\mu\nu}$ the energy-momentum tensor of the field, and p^ν the 4-momentum of the electron.

The average Upsilon parameter in a bunch of linear colliders is [3]

$$\Upsilon_{av} = \frac{5}{6}\frac{N_e r_e^2\gamma}{\alpha\sigma_z(\sigma_x+\sigma_y)}, \tag{12}$$

and for the above parameters, Υ_{av} is about 631. For example, in the NLC we find $\Upsilon_{av} \sim 0.1$ to 1.0.

The beamstrahlung radiation formula was first derived by Sokolov and Ternov [6]. The Sokolov-Ternov spectrum formula is [3]

$$\frac{dW_\gamma}{d\omega} = \frac{\alpha}{\sqrt{3}\pi\gamma^2}F_{BS}, \tag{13}$$

with

$$F_{BS} = \int_\xi^\infty K_{5/3}(\xi')d\xi' + \frac{y^2}{1-y}K_{2/3}(\xi), \tag{14}$$

where K_ν is the modified Bessel function and

$$\xi = \frac{2\omega}{3\Upsilon(E-\omega)} = \frac{\omega}{\omega_c}\frac{1}{1-\omega/E} = \frac{2}{3\Upsilon}\frac{y}{1-y} \qquad (y = \frac{\omega}{E}), \tag{15}$$

where the radiated photon energy is ω and we define $W_\gamma = dw_\gamma/dt$ [s^{-1}] where ω_γ is the probability of photon emission. The first term in Eq. (14) is the classical formula for synchrotron radiation.

The Sokolov-Ternov spectrum is shown in Fig. 1. The energy of the electron beam is 2.5 TeV. In the classical regime $\Upsilon \ll 1$, the second term is small and the spectrum is the same as the classical formula. In the quantum regimes $\Upsilon > 1$, the second term in Eq. (14) is larger than the first term in it at $y = 1$ and the first term is still dominant at low energies. The probability of photon emission is in proportion to $\Upsilon^{2/3}$ for $\Upsilon > 1$ in Fig. 1.

For more convenient expression, the approximate formula of the Sokolov-Ternov spectrum in Eq. (14) is

$$F_{BS,approx.} = \frac{5\pi}{3\Gamma(1/3)}(\xi^{-2/3} + \Upsilon\xi^{2/5})\exp(-\xi), \tag{16}$$

where $\Gamma(1/3) = 2.67894$. This formula can be used for arbitrary Υ parameter. We use it later in this paper.

The Sokolov-Ternov power spectrum is defined as

$$P(\omega) = \frac{dW_\gamma}{d\omega}\omega = \frac{1}{E}\frac{dW_\gamma}{dy}\omega \ [\mathrm{s}^{-1}], \tag{17}$$

and the Sokolov-Ternov power spectrum is shown in Fig. 2. From this figure, we can see larger energy loss of the beams with larger probability in the deep quantum regime.

When we assume the Gaussian bunches, the average number of emitted photons per electron n_γ is [3]

$$n_\gamma \approx 2.59 \left[\frac{\alpha\sigma_z\Upsilon}{\lambda\!\!\!^{-}_e\gamma}\right] U_0(\Upsilon), \tag{18}$$

where

$$U_0(\Upsilon) \approx \frac{1}{(1+\Upsilon^{2/3})^{1/2}}. \tag{19}$$

The relative energy loss in the case of the Gaussian bunch is [3]

$$\delta_E \approx 1.20 \left[\frac{\alpha\sigma_z\Upsilon}{\lambda\!\!\!^{-}_e\gamma}\right] \Upsilon U_1(\Upsilon), \tag{20}$$

where

$$U_1(\Upsilon) \approx \frac{1}{\left[1+(1.5\Upsilon)^{2/3}\right]^2}. \tag{21}$$

For our case, we find $n_\gamma = 0.73$ and $\delta_E = 0.19$. The beam-beam parameters given by the CAIN simulation are listed in Table III. From simulation, we get $n_\gamma = 0.91$ and $\delta_E = 0.17$. Figure 3 shows the relative energy loss distribution as a function of Υ and σ_z. The energy of the electron beam is 2.5 TeV. If we assume the small bunch length in order to suppress the energy loss from beamstrahlung, we can apply a large Υ parameter.

Figure 4 shows the scatter plot of the energy and the scattering angle of photons. The one dot exhibits 15000 real particles. The beamstrahlung photons generated by the initial beams with energy of 2.5 TeV occupy the band below 0.2 mrad, roughly. This angle corresponds to the disruption angle $\theta_0 = 0.16$ mrad in Eq.(8). The photons with the angle larger than 0.2 mrad are generated through multiple beamstrahlung by the initial beams or the coherent pair-created particles to be discussed later, because the number of the coherent pair creation is very large. The maximum angle of the photons corresponds to that of the opposite charge particles in the oncoming beam in Eq.(10). The angle-energy correlation, shown more remarkably above the lower band, is due to the fact that the lower the energy of the radiating particle, the larger the angle it is deflected by the beam field, and the larger the angle of the radiated photon.

B. Coherent pairs

Due to high Υ, the coherent e^+e^- pairs which are created by beamstrahlung photons traveling in the strong field of the opposite beams are candidates for the source of backgrounds. The total number of the coherent pairs per primary particle is [3]

$$n_b = \left[\frac{\alpha\sigma_z\Upsilon}{\gamma\lambda\!\!\!^{-}_e}\right]^2 \Xi(\Upsilon), \tag{22}$$

where

$$\Xi(\Upsilon) = \begin{cases} (7/128)\exp(-16/3\Upsilon) & (\Upsilon \lesssim 1) \\ 0.295\Upsilon^{-2/3}(\ln\Upsilon - 2.488) & (\Upsilon \gg 1). \end{cases} \tag{23}$$

For the above parameters, we find $n_b = 0.094$. From simulation, $n_b = 0.11$ is given. Since the number of the coherent pairs per bunch crossing is about 3.0×10^7 and is very large, we need to estimate the number of the coherent pair particles with the large inherent angle.

The probability of the coherent pair creation as a function of θ, the inherent angle between the photon and the $(\mathrm{v}, \dot{\mathrm{v}})$ plane of the secondary particle, and the energy ϵ of a pair-created particle (either e^+ or e^-) per unit time can be derived from [13]

$$\frac{d^3n}{dtd\theta d\epsilon} = \frac{8\alpha}{3\pi^2}\frac{\epsilon m}{\omega^2\chi}\cosh^2 u\cosh^2 v \\ \times\{K_{1/3}^2(\eta) + \cosh^2 u(2\cosh^2 v - 1)[K_{1/3}^2(\eta) + K_{2/3}^2(\eta)]\}, \tag{24}$$

where $\cosh^2 u = 1 + \gamma_\epsilon^2\theta^2$, $\gamma_\epsilon = \epsilon/m$, $\cosh^2 v = \omega^2/[4\epsilon(\omega - \epsilon)]$, $\eta = (4/3\chi)\cosh^2 v\cosh^3 u$, $\chi = (\omega/E)\Upsilon$, ω and E the energies of the beamstrahlung photon and the primary particle.

The probability of the coherent pair creation with $\epsilon \geq \epsilon_0$ and $|\cos\theta| \leq \cos\theta_0$ is

$$\frac{dn(\epsilon_0, \theta_0)}{dt} = \int_{\epsilon_0}^{\omega} d\epsilon \int_{\theta_0}^{\pi-\theta_0} d\theta \frac{d^3n}{dtd\theta d\epsilon}. \tag{25}$$

The number of the coherent pairs with $\epsilon \geq \epsilon_0$ and $|\cos\theta| \leq \cos\theta_0$ per primary particle is

$$\begin{aligned} n_b(\epsilon_0, \theta_0) &= \int\int_{t_2>t_1}\int_0^{E_0} dt_2 dt_1 d\omega \frac{dw_\gamma}{d\omega dt_1}\frac{dn(\epsilon_0, \theta_0)}{dt_2} \\ &= \frac{3\sigma_z^2}{2}\int_0^{E_0} d\omega \frac{dw_\gamma}{d\omega} n(\epsilon_0, \theta_0) \\ &= \frac{20\sqrt{3}}{9\Gamma(1/3)\pi^2}\frac{\alpha^2 m\sigma_z^2}{\gamma^2}\int_0^{E_0} d\omega \left(\xi^{-2/3} + \Upsilon\xi^{2/5}\right)\exp(-\xi) \\ &\times \int_{\epsilon_0}^{\omega} d\epsilon \int_{\theta_0}^{\pi-\theta_0} d\theta \frac{\epsilon}{\omega^2\chi}\cosh^2 u\cosh^2 v \\ &\times \left\{K_{1/3}^2(\eta) + \cosh^2 u\left(2\cosh^2 v - 1\right)\left[K_{1/3}^2(\eta) + K_{2/3}^2(\eta)\right]\right\}. \end{aligned} \tag{26}$$

Here we consider the case of longitudinally uniform beams with the small disruption and the constant Υ along the photon path and we can replace $\int\int dt_1 dt_2$ by $3\sigma_z^2/2$ [3]. The number of the coherent pair creation with $\epsilon_0 = 0$ GeV and $\theta_0 = 0$ is $n_b(\epsilon_0, \theta_0) = 0.091$ from Eq.(26).

The number of the coherent pair particles per bunch crossing with $\epsilon \geq \epsilon_0$ and $|\cos\theta| \leq \cos\theta_0$ using Eq.(26), are listed in Table IV. The number of the pair particles with the inherent angle larger than 1 mrad and the energy larger than 100 MeV is less than 1. Since the inherent angle of the coherent pairs is correspond to $1/\gamma_\epsilon$, so that the situation is very similar to beamstrahlung, the larger the energy of the pairs and the smaller the inherent angle of the pairs. Comparing these angles with the disruption angles in Eqs.(9) and (10), we can understand that the inherent angle of the coherent pairs is negligible.

Figure 5 shows the scatter plot of the energy and the scattering angle of the coherent pairs and the initial beam particles. The one dot exhibits 15000 real particles. The initial beam particles are concentrated mostly in the area near full energy. We notice the split of two bands in the lower energy region. The band with larger angle corresponds to the opposite sign pair partners. The band with smaller angle corresponds to the same sign partners. The solid and dashed lines indicate the maximum angles of the opposite and same charge particles in Eqs.(10) and (9). The deflection angle for the opposite sign pair particle is up to 100 mrad with energy as low as several hundred MeV.

In Fig. 6, the scatter plot of the scattering angle and the transverse momentum of the coherent pairs and the initial beam particles is shown. The one dot exhibits 15000 real particles. Here again the band with larger angle corresponds to the opposite sign pair partners.

In the deep quantum regime, coherent pairs can also be produced from virtual photons (as opposed to real photons from beamstrahlung) through a process known as trident cascade. The current version of CAIN code does not include this process, but the total number of the trident cascade per primary particle can be estimated with a simple formula [3,14]

$$n_v = \left(\frac{\alpha\sigma_z}{\gamma\lambda_e}\Upsilon\right)\Omega(\Upsilon), \tag{27}$$

where

$$\Omega(\Upsilon) \sim 0.23\alpha\ln\Upsilon,\ \Upsilon \gg 1, \tag{28}$$

where γ_E is Euler's constant and for the above parameters, n_v is about 0.026. In our parameters, this production rate is smaller than that of the coherent pair production from real beamstrahlung photons. Recently Thompson and Chen have reexamined this process and found that there is much less than one trident pair per bunch crossing with a large outgoing angle in our parameters [15].

C. Incoherent pairs

In addition to coherent pairs produced in collective beam field, the incoherent pairs can be created through individual particle scattering processes. These are Breit-Wheeler ($\gamma\gamma \rightarrow e^+e^-$), Bethe-Heitler ($e\gamma \rightarrow ee^+e^-$), and Landau-Lifshitz ($ee \rightarrow eee^+e^-$) processes by the interactions both real (beamstrahlung) and virtual photons.

The spectrum for the real beamstrahlung photons is given by the integration of Eq.(16) over collision time

$$n_b(y) = \int_{-\sqrt{3}\sigma_z}^{\sqrt{3}\sigma_z} \frac{dW_\gamma}{dy} dt \tag{29}$$

$$= \frac{10}{3\Gamma(1/3)} \left(\frac{\alpha\sigma_z}{\gamma \lambda\!\!\!^{-}_e}\right) \left(\xi^{-2/3} + \Upsilon\xi^{2/5}\right) \exp(-\xi). \tag{30}$$

Virtual photons are emitted by the collisions of individual particles. The spectrum of the virtual photons from electron beams is derived by the well-known equivalent photon approximation [3]

$$n_v(y) = \frac{2\alpha}{\pi}\frac{1}{y} \ln\left(\frac{1}{y}\right). \tag{31}$$

The differential cross section for Breit-Wheeler (BW) process with the scattering angle θ in the lab. frame is [3]

$$\sigma_{\gamma\gamma}(y_1, y_2) = \frac{d\sigma_{\gamma\gamma}}{d\cos\theta} \simeq \frac{\pi r_e^2}{\gamma^2 y_1 y_2} \frac{1}{1-\cos^2\theta}, \tag{32}$$

where y_1 and y_2 are the energy fractions of two photons divided by the initial beam energy. Since the dominant contribution to the BW cross section is associated with the $\theta_0 \sim 1/(\gamma\sqrt{y_1 y_2})$, the cross section of BW process is approximately given by [3]

$$\sigma_{\rm BW}(y_1, y_2) = \frac{\pi r_e^2}{2\gamma^2 y_1 y_2} \ln(4\gamma^2 y_1 y_2). \tag{33}$$

The effective cross section for BW process including two beamstrahlung spectra is

$$\sigma_{\rm BW} = \frac{1}{4}\int_{1/\gamma^2}^{1} dy_1 \int_{1/(\gamma^2 y_1)}^{1} dy_2\; n_b(y_1) n_b(y_2) \sigma_{\rm BW}(y_1, y_2) \tag{34}$$

$$= \frac{25\pi}{18\Gamma(1/3)^2} \left(\frac{\alpha r_e \sigma_z}{\gamma^2 \lambda\!\!\!^{-}_e}\right)^2 \int_{1/\gamma^2}^{1} dy_1 \int_{1/(\gamma^2 y_1)}^{1} dy_2 \times \left(\xi_1^{-2/3} + \Upsilon\xi_1^{2/5}\right)\left(\xi_2^{-2/3} + \Upsilon\xi_2^{2/5}\right) \exp(-\xi_1 - \xi_2) \ln(4\gamma^2 y_1 y_2)/(y_1 y_2), \tag{35}$$

where

$$\xi_1 = \frac{2}{3\Upsilon}\frac{y_1}{1-y_1},\; \xi_2 = \frac{2}{3\Upsilon}\frac{y_2}{1-y_2}. \tag{36}$$

Here the factor 1/4 is the effective collision time for the beamstrahlung photons and the threshold condition for pair creation is that $m = \sqrt{\omega_1\omega_2}$ and the lower bound for the photon energy y_2 with a fixed photon energy y_1 is $y_2 = 1/(\gamma^2 y_1)$.

The effective cross section for Bethe-Heitler (BH) process including the beamstrahlung and virtual photon spectra is

$$\sigma_{\rm BH} = \int_{1/\gamma^2}^{1} dy_1 \int_{1/(\gamma^2 y_1)}^{1} dy_2 \; n_b(y_1) n_v(y_2) \sigma_{\rm BW}(y_1, y_2) \tag{37}$$

$$= \frac{10}{3\Gamma(1/3)} \left(\frac{\alpha^2 r_e^2 \sigma_z}{\gamma^3 \lambda\!\!\!^{-}_e}\right) \int_{1/\gamma^2}^{1} dy_1 \int_{1/(\gamma^2 y_1)}^{1} dy_2$$

$$\times \left(\xi_1^{-2/3} + \Upsilon \xi_1^{2/5}\right) \exp(-\xi_1) \ln(1/y_2) \ln(4\gamma^2 y_1 y_2)/(y_1 y_2^2). \tag{38}$$

The effective cross section for Landau-Lifshitz (LL) process including two virtual photon spectra is

$$\sigma_{\rm LL} = \int_{1/\gamma^2}^{1} dy_1 \int_{1/(\gamma^2 y_1)}^{1} dy_2 \; n_v(y_1) n_v(y_2) \sigma_{\rm BW}(y_1, y_2) \tag{39}$$

$$= \frac{2}{\pi} \left(\frac{\alpha r_e}{\gamma}\right)^2 \int_{1/\gamma^2}^{1} dy_1 \int_{1/(\gamma^2 y_1)}^{1} dy_2$$

$$\times \ln(1/y_1) \ln(1/y_2) \ln(4\gamma^2 y_1 y_2)/(y_1 y_2)^2. \tag{40}$$

The effective cross section and the number of the incoherent pair creation are listed in Table. V. The number of the BH and LL processes are several ten thousands and that of the BW process is much smaller than two processes. The number of the incoherent pairs is more than 2 orders of magnitude below that of the coherent pairs. From simulation, the total number of the incoherent pairs per bunch crossing is about 1.2×10^4 and this number is smaller than the results by the formulas due to the effect of the geometrical reduction [3]. Here we assume the effective cross section including the effect of the geometrical reduction, $\bar{\sigma} = \sigma - \sigma'$, where σ and σ' are the effective and cut-off cross sections. The equivalent photon spectrum associated with the cut-off cross section σ' is [3]

$$n_v^{cut}(y) = \frac{2\alpha}{\pi} \frac{dy}{y} \ln\left(\frac{\lambda\!\!\!^{-}_e / 2\sigma_{x(y)}}{y}\right). \tag{41}$$

The cut-off cross section σ' for the BH and LL processes can be derived by inserting $n_v^{cut}(y)$ into Eqs. (37) and (39) and the upper bounds of the y-integrations have to be replaced by $\lambda\!\!\!^{-}_e/2\sigma_{x(y)}$. Table V lists the effective cross section and the number of the incoherent pair creation including the effect of the geometrical reduction. Because of the geometrical reduction, the pair backgrounds from the BH and LL processes are less serious.

In order to calculate the number of the incoherent pair particles with the transverse momentum divided by γm, $p_\perp \geq p_{\perp 0}$, and the out-coming angle $|\cos\theta| \leq \cos\theta_0$, we introduce the following parameters. The initial photon energies are limited by [3]

$$y_\pm = \frac{p_\perp}{2} \sqrt{\frac{1 \pm \cos\theta}{1 \mp \cos\theta}}. \tag{42}$$

For any given value of $y_2 \geq y_1$, the lower bound for y_1 is [3]

$$y_b = \frac{y_2 y_+}{y_2 - y_-}. \tag{43}$$

The partial cross section with $p_\perp \geq p_{\perp 0}$ and $|\cos\theta| \leq \cos\theta_0$ for BW process is

$$\sigma_{\rm BW}(p_{\perp 0}, \cos\theta_0) = \frac{1}{4} \int_{-\cos\theta_0}^{+\cos\theta_0} d\cos\theta \int_{y_-}^{\infty} dy_2 \int_{y_b}^{\infty} dy_1 n_b(y_1) n_b(y_2) \sigma_{\gamma\gamma}(y_1, y_2) \tag{44}$$

$$= \frac{25\pi}{9\Gamma(1/3)^2} \left(\frac{\alpha r_e \sigma_z}{\gamma^2 \lambda\!\!\!^{-}_e}\right)^2 \int_{-\cos\theta_0}^{+\cos\theta_0} d\cos\theta \int_{y_-}^{\infty} dy_2 \int_{y_b}^{\infty} dy_1$$

$$\times \left(\xi_1^{-2/3} + \Upsilon \xi_1^{2/5}\right) \left(\xi_2^{-2/3} + \Upsilon \xi_2^{2/5}\right) \exp(-\xi_1 - \xi_2) \frac{1}{y_1 y_2} \frac{1}{1 - \cos^2\theta}. \tag{45}$$

The partial cross section with $p_\perp \geq p_{\perp 0}$ and $|\cos\theta| \leq \cos\theta_0$ for BH process is

$$\sigma_{\rm BH}(p_{\perp 0}, \cos\theta_0) = \int_{-\cos\theta_0}^{+\cos\theta_0} d\cos\theta \int_{y_-}^{\infty} dy_1 \int_{y_b}^{\infty} dy_2 n_b(y_1) n_v(y_2) \sigma_{\gamma\gamma}(y_1, y_2) \tag{46}$$

$$= \frac{20}{3\Gamma(1/3)} \left(\frac{\alpha^2 r_e^2 \sigma_z}{\gamma^3 \lambda\!\!\!^{-}_e}\right) \int_{-\cos\theta_0}^{+\cos\theta_0} d\cos\theta \int_{y_-}^{\infty} dy_1 \int_{y_b}^{\infty} dy_2$$

$$\times \left(\xi_1^{-2/3} + \Upsilon \xi_1^{2/5}\right) \exp(-\xi_1) \ln(1/y_2) \frac{1}{y_1 y_2^2} \frac{1}{1 - \cos^2\theta} \tag{47}$$

The partial cross section with $p_\perp \geq p_{\perp 0}$ and $|\cos\theta| \leq \cos\theta_0$ for LL process is

$$\sigma_{\rm LL}(p_{\perp 0}, \cos\theta_0) = \int_{-\cos\theta_0}^{+\cos\theta_0} d\cos\theta \int_{y_-}^{\infty} dy_1 \int_{y_b}^{\infty} dy_2 n_v(y_1) n_v(y_2) \sigma_{\gamma\gamma}(y_1, y_2) \tag{48}$$

$$= \frac{4}{\pi}\left(\frac{\alpha r_e}{\gamma}\right)^2 \int_{-\cos\theta_0}^{+\cos\theta_0} d\cos\theta \int_{y_-}^{\infty} dy_1 \int_{y_b}^{\infty} dy_2$$

$$\times \ln(1/y_1)\ln(1/y_2)\frac{1}{(y_1 y_2)^2}\frac{1}{1-\cos^2\theta}. \tag{49}$$

Table VI lists the partial cross section and the number of the incoherent pair particles with the transverse momentum $p_t \geq p_{t_0}$ and $|\cos\theta| \leq \cos\theta_0$. The all number of the case (b) $\theta_0 = 100$ mrad and $p_{t_0} = 50$ MeV are smaller than 1. From the table, we can reduce the backgrounds from the incoherent pairs by applying the adequate cuts.

Figure 7 shows the scatter plot of the energy and the scattering angle of the incoherent pairs. The one dot exhibits one real particle. The two bands correspond to the opposite sign partners in the larger angle region and the same sign partners in the smaller angle region. The scatter plot of the energy and the scattering angle of the incoherent pairs is shown in Fig. 8. The one dot exhibits one real particle. Similarly the band with larger angle on the right corresponds to opposite sign partners.

IV. LUMINOSITY DISTRIBUTION

In this section, we introduce the luminosity distribution of a 5 TeV linear collider with $\Upsilon = 631$. Here we do not use the spectrum of the virtual photons in Eq.(31). The spectrum of the virtual photons from electron beams is given by the well-known equivalent photon approximation [16]

$$n_v'(y) = \frac{\alpha}{2\pi}\left(\frac{1+(1-y)^2}{y}\ln\left[\frac{(1-y)P_{\rm max}^2}{m^2 y^2}\right] - \frac{2(1-y)}{y}\right), \tag{50}$$

where y and $P_{\rm max}^2$ denote the energy fraction taken by the photon from the electron and the maximum photon virtuality. In this article, the photon virtuality was restricted to $P_{\rm max}^2 = 0.01$ GeV^2 [16].

Figure 9 shows the luminosity distribution of a 5 TeV linear collider with $\Upsilon = 631$. The luminosity distribution of the e^+e^-, $e\gamma$, and $\gamma\gamma$ collisions in Fig. 9 have been calculated by using the CAIN code. The maximum energy of the collisions between beamstrahlung photons reaches near $\sqrt{s} = 5$ TeV due to the large Υ parameter. Using the analytic formula of Eq.(50), the luminosity of the $\gamma^*\gamma^*$ collisions (γ^* denotes virtual photons.) was calculated by

$$L_{\gamma^*\gamma^*}(\sqrt{s}) = L_{ee}\int_0^1\int_0^1 n_v'(y_1) n_v'(y_2)\delta\left(s - 4y_1 y_2 E_0^2\right) dy_1 dy_2, \tag{51}$$

where L_{ee} is the total luminosity of the e^+e^- collisions. The collisions between virtual photons over $\sqrt{s} > 1$ TeV is negligible in comparison with other collisions. It is needless to say that we will have to consider the superposition of the beamstrahlung and virtual photon spectrums.

The total luminosity of an e^+e^- linear collider with the laser drive at $\sqrt{s}_{e^+e^-} = 5$ TeV are listed in Table VII. There is about a half of the total luminosity of the e^+e^- collisions with $\sqrt{s} > 4.975$ TeV and it presents a narrow width for precision study.

Here, z and η are defined as

$$z = \sqrt{s}/2E_0, \tag{52}$$

$$\eta = \ln\sqrt{E_1/E_2}, \tag{53}$$

where E_1 and E_2 are the energies of left- and right-moving particles, respectively.

The e^+e^- luminosity distribution of a 5 TeV e^+e^- linear collider with $\Upsilon = 631$ are shown in Fig. 10 and 11. In Fig. 10, the peak of the luminosity is seen at $E_1 = E_2 = 2.5$ TeV and we can see two walls of the collisions between the full energy and degraded particles at $E_1 = 2.5$ TeV or $E_2 = 2.5$ TeV. Similarly, the same walls are seen in Fig. 11. Since the parameter η presents the boost effects of the frame, the events from the peak of the luminosity at $\eta = 0$ are occurred at rest.

The $e\gamma$ luminosity distribution of a 5 TeV e^+e^- linear collider with $\Upsilon = 631$ are shown in Fig. 12 and 13. In Fig. 12, the peak of the luminosity at $E_1 = 0$ TeV and $E_2 = 2.5$ TeV is seen and we can see two walls at $E_1 = 0$ TeV or $E_2 = 2.5$ TeV. The events from the $e\gamma$ collision at $z < 1$ are boosted in Fig. 13.

The $\gamma\gamma$ luminosity distribution of a 5 TeV e^+e^- linear collider with $\Upsilon = 631$ are shown in Fig. 14 and 15. In Fig. 14, the peak of the luminosity at $E_1 = 0$ TeV and $E_2 = 0$ TeV is seen and we can see two walls at $E_1 = 0$ TeV or $E_2 = 0$ TeV. The $\gamma\gamma$ collisions at small z are widely distributed on the η axis in Fig. 15.

Since the events from the e^+e^- and $e\gamma$ collisions at $z < 1$ are boosted from the two-dimensional plots and the $\gamma\gamma$ collisions at $z = 1$ are much smaller than e^+e^- collisions at $z = 1$, the 5 TeV e^+e^- linear collider with $\Upsilon = 631$ has a good potential for precision study of e^+e^- collisions.

V. SUMMARY

In this paper, we have investigated the QED backgrounds induced by the beam-beam interaction in a 5 TeV e^+e^- linear collider, especially in the deep quantum regime $\Upsilon \gg 1$. In the deep quantum regime, the IP environment is different from that in the classical and intermediate regimes ($\Upsilon \lesssim 1$). First, the beamstrahlung photons at higher energy in $\Upsilon \gg 1$ are radiated and the initial beams lose larger energy. Second, the coherent pairs in $\Upsilon \gg 1$ are largely produced. In order to reduce the effects, we take an effect of quantum suppression of beamstrahlung due to the very short bunch length. For the IR design of linear collider, the electron-positron pair production from real and virtual photons in the arbitrary Υ regime is derived. From the formulas of the coherent and incoherent pair creation, we have estimated the pair backgrounds with the large inherent angle in a 5 TeV e^+e^- linear collider. For particle physics experiment, the e^+e^-, $e\gamma$, and $\gamma\gamma$ luminosity distribution in a 5 TeV e^+e^- linear collider are evaluated with simulation. From the analytical and simulated estimation, we can understand that the approach of quantum suppression of beamstrahlung is acceptable for the experiments of high energy physics.

ACKNOWLEDGMENTS

We wish to extend many thanks to S. Chattopadhyay, P. Chen, K.-J. Kim, H. Murayama, J. Siegrist, T. Tajima, and K. Yokoya for helpful discussions. This work was supported in part by the U.S. Department of Energy under Contract No. DE-AC03-76SF00098.

TABLE I. Beam parameters of an e^+e^- linear collider with the laser drive at $\sqrt{s}_{e^+e^-}$=5 TeV [10].

Υ	P_b (MW)	$N(10^8)$	f_c (kHz)	ϵ_x/ϵ_y (nm)	$\beta_x/\beta_y(\mu$m)	σ_x/σ_y (nm)	σ_z (μm)
631	20	1.6	156	25/25	62/62	0.56/0.56	1

TABLE II. Parameters given by the formulas.

Υ	D_y	θ_0 (mrad)	n_γ	δ_E	n_b	n_v	L_0 (10^{35}cm^{-2}s^{-1})
631	0.29	0.16	0.73	0.19	0.094	0.026	1

TABLE III. Parameters given by the CAIN simulation.

n_γ	δ_E	σ_e/E_0	n_b
0.91	0.17	0.36	0.11

TABLE IV. The number of the coherent pair particles per bunch crossing with $\epsilon \geq \epsilon_0$ and $|\cos\theta| \leq \cos\theta_0$. The cut-offs of the angle and the energy are (a) $\theta_0 = 1$ mrad and $\epsilon_0 = 0.1$ GeV, (b) $\theta_0 = 500$ μrad and $\epsilon_0 = 1$ GeV, (c) $\theta_0 = 150$ μrad and $\epsilon_0 = 10$ GeV, respectively.

	(a)	(b)	(c)
Number of particles per bunch crossing	0.61	110	13

TABLE V. The effective cross section and the number of the incoherent pair creation. Those including the effect of the geometrical reduction are also calculated.

	BW	BH	LL
Effective cross section σ (cm^2)	2.8×10^{-29}	5.0×10^{-26}	2.7×10^{-26}
Number of pairs per bunch crossing	20	3.5×10^4	1.9×10^4
Geom. cross section $\bar{\sigma}$ (cm^2)	2.8×10^{-29}	1.5×10^{-26}	1.7×10^{-26}
Number of pairs per bunch crossing (Geom.)	20	1.1×10^4	1.2×10^4
$\bar{\sigma}/\sigma$	1.0	0.30	0.61

TABLE VI. The partial cross section and the number of the incoherent pair particles with $p_t \geq p_{t_0}$ and $|\cos\theta| \leq \cos\theta_0$. The cut-offs of the angle and the transverse momentum are (a) $\theta_0 = 10$ mrad and $p_{t_0} = 100$ MeV, (b) $\theta_0 = 100$ mrad and $p_{t_0} = 50$ MeV, (c) $\theta_0 = 500$ mrad and $p_{t_0} = 10$ MeV, respectively.

	BW	BH	LL
Partial cross section (cm^2)			
(a)	1.7×10^{-32}	2.8×10^{-31}	2.3×10^{-31}
(b)	2.4×10^{-32}	3.4×10^{-31}	6.5×10^{-31}
(c)	9.3×10^{-32}	2.1×10^{-30}	1.0×10^{-29}
Number of particles per bunch crossing			
(a)	2.4×10^{-2}	0.39	0.33
(b)	3.4×10^{-2}	0.48	0.93
(c)	0.13	3.1	15

TABLE VII. Total luminosity of an e^+e^- linear collider with the laser drive at $\sqrt{s}_{e^+e^-}$=5 TeV (Unit 10^{35}cm^{-2}s^{-1}).

	L_{ee}	L_{ee} ($\sqrt{s} > 4.975$ TeV)	$L_{e\gamma}$	$L_{\gamma\gamma}$	$L_{\gamma^*\gamma^*}$ ($\sqrt{s}$ >1 GeV)
Total	1.3	0.61	0.49	0.21	0.34

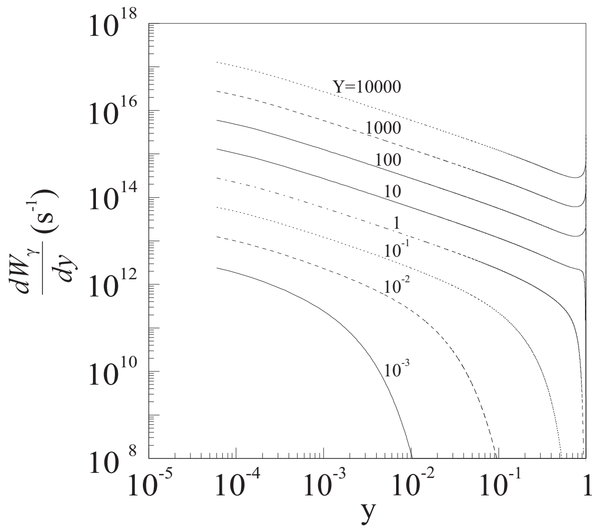

FIG. 1. Sokolov-Ternov spectrum. The energy of the electron beam is 2.5 TeV. From bottom to top, Υ parameters are $10^{-3}, 10^{-2}, 10^{-1}, 1, 10, 100, 1000, 10000$, respectively.

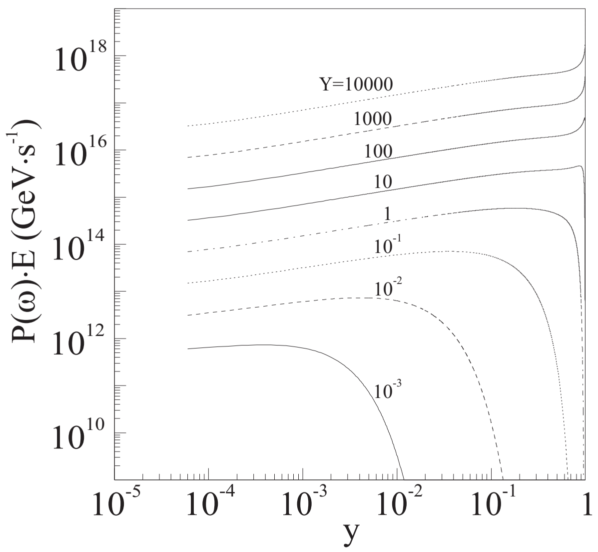

FIG. 2. Sokolov-Ternov power spectrum. The energy of the electron beam is 2.5 TeV. From bottom to top, Υ parameters are $10^{-3}, 10^{-2}, 10^{-1}, 1, 10, 100, 1000, 10000$, respectively.

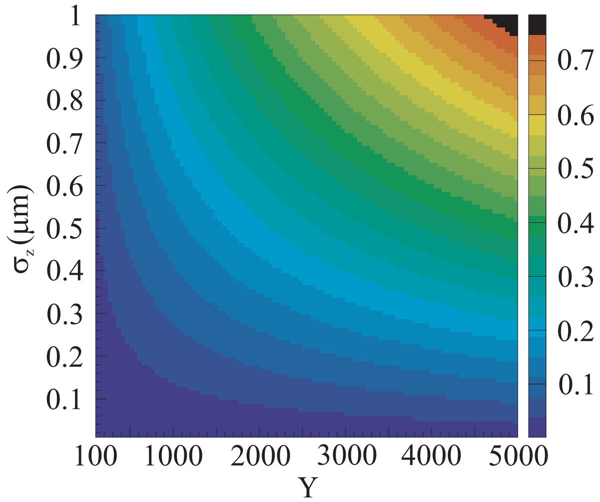

FIG. 3. Relative energy loss distribution as a function of Υ and σ_z. The energy of the electron beam is 2.5 TeV.

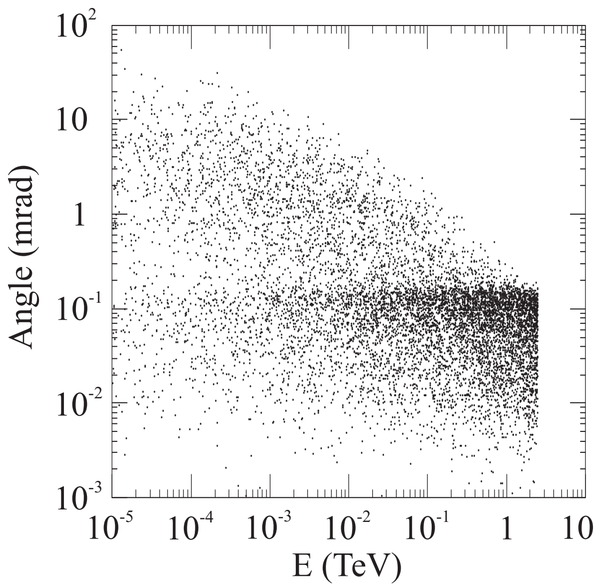

FIG. 4. Scatter plot of the energy and the scattering angle of the photons. The one dot exhibits 15000 real particles.

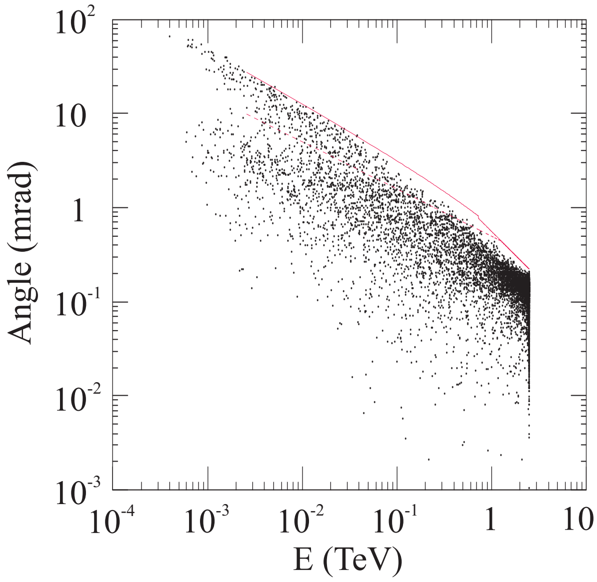

FIG. 5. Scatter plot of the energy and the scattering angle of the coherent pairs and the initial beam particles. The one dot exhibits 15000 real particles. The solid and dashed lines indicate the maximum angles of the opposite and same charge particles in Eqs.(10) and (9).

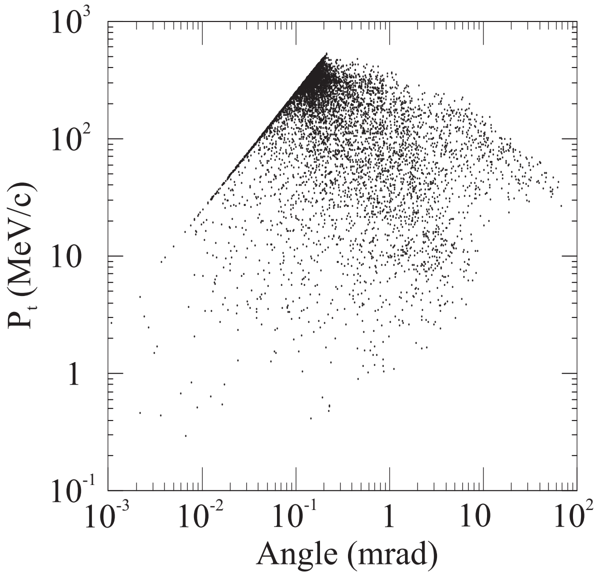

FIG. 6. Scatter plot of the scattering angle and the transverse momentum of the coherent pairs and the initial beam particles. The one dot exhibits 15000 real particles.

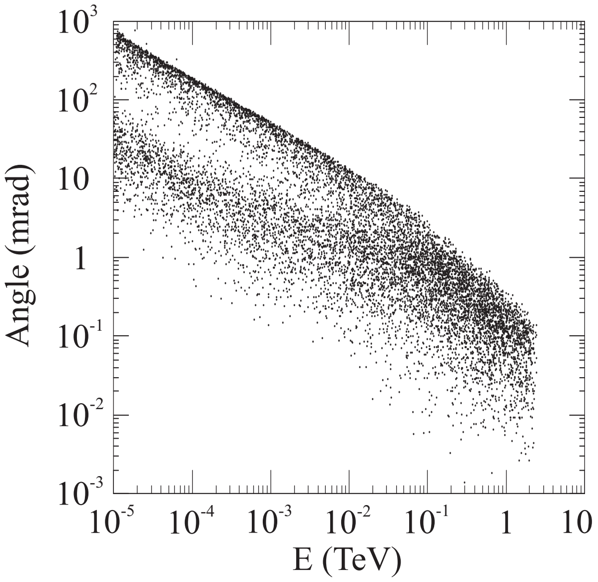

FIG. 7. Scatter plot of the energy and the scattering angle of the incoherent pairs. The one dot exhibits one real particle.

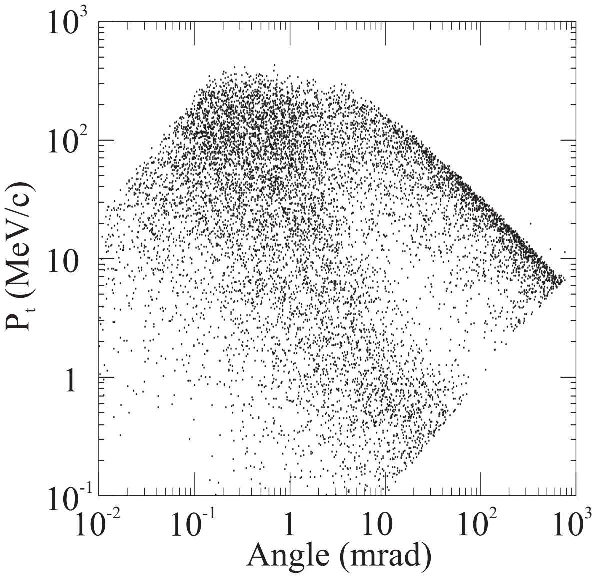

FIG. 8. Scatter plot of the scattering angle and the transverse momentum of the incoherent pairs. The one dot exhibits one real particle.

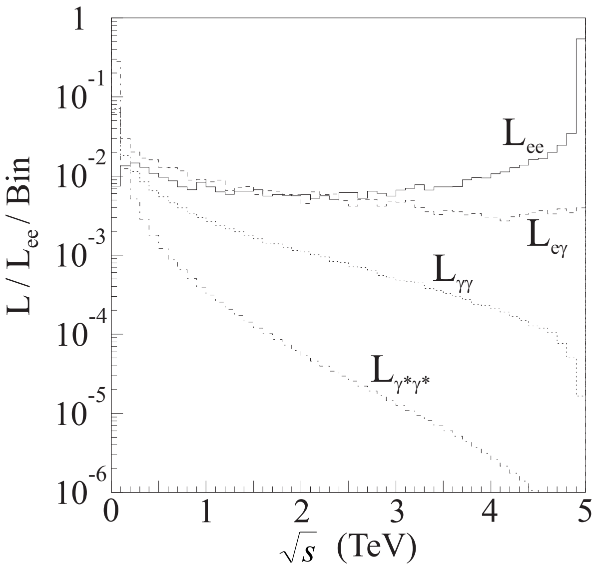

FIG. 9. Luminosity distribution of a 5 TeV e^+e^- linear collider with $\Upsilon = 631$. The vertical axis is normalized by the total luminosity of the e^+e^- collisions. The bin size is 100 GeV.

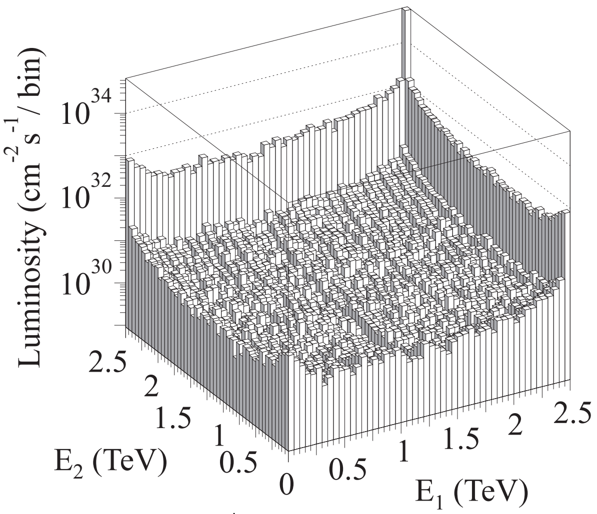

FIG. 10. The e^+e^- luminosity distribution of a 5 TeV e^+e^- linear collider with $\Upsilon = 631$. The vertical axis is $d^2L_{e^+e^-}/dE_1dE_2$ in units of cm^{-2}s^{-1}/bin. The bin size is 50 GeV$\times$50 GeV.

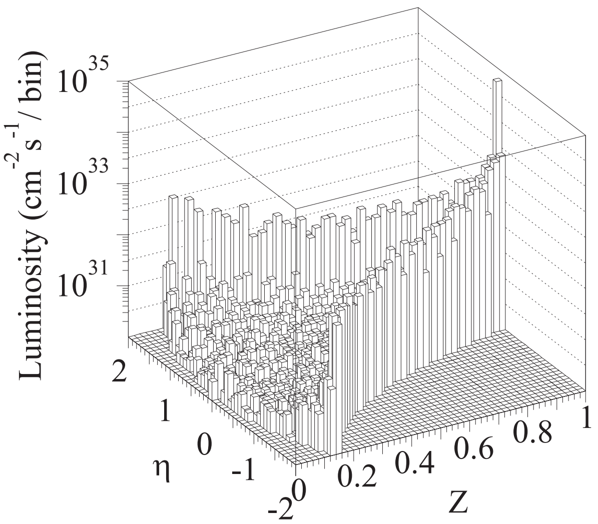

FIG. 11. The e^+e^- luminosity distribution of a 5 TeV e^+e^- linear collider with $\Upsilon = 631$. The vertical axis is $d^2L_{e^+e^-}/dzd\eta$ in units of $\mathrm{cm}^{-2}\mathrm{s}^{-1}$/bin. The bin size $\Delta z \times \Delta\eta$ is 0.02×0.1.

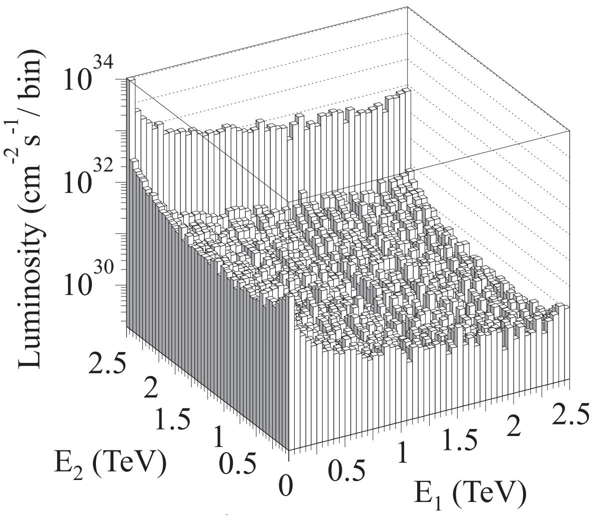

FIG. 12. The $e\gamma$ luminosity distribution of a 5 TeV e^+e^- linear collider with $\Upsilon = 631$. The energies of the photon and the electron are E_1 and E_2, respectively. The vertical axis is $d^2L_{e\gamma}/dE_1E_2$ in units of $\mathrm{cm}^{-2}\mathrm{s}^{-1}$/bin. The bin size is 50 GeV$\times$50 GeV.

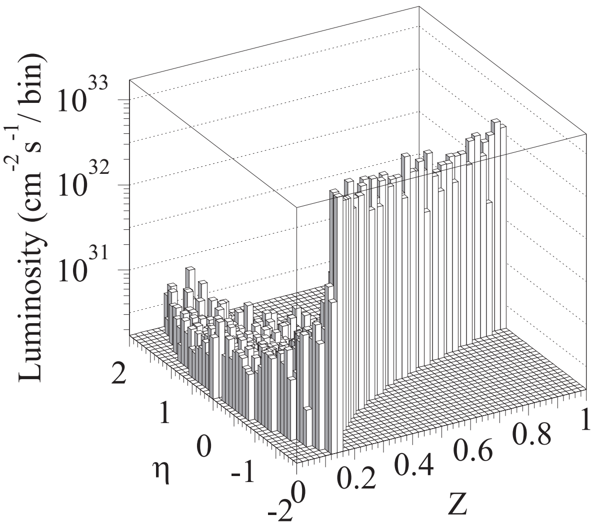

FIG. 13. The $e\gamma$ luminosity distribution of a 5 TeV e^+e^- linear collider with $\Upsilon = 631$. The vertical axis is $d^2L_{e\gamma}/dzd\eta$ in units of $\mathrm{cm}^{-2}\mathrm{s}^{-1}$/bin. The bin size $\Delta z \times \Delta\eta$ is 0.02×0.1.

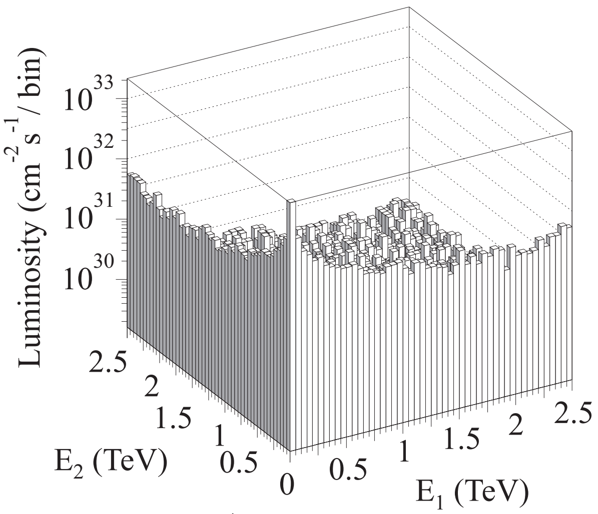

FIG. 14. The $\gamma\gamma$ luminosity distribution of a 5 TeV e^+e^- linear collider with $\Upsilon = 631$. The vertical axis is $d^2L_{\gamma\gamma}/dE_1dE_2$ in units of $\mathrm{cm}^{-2}\mathrm{s}^{-1}$/bin. The bin size is 50 GeV$\times$50 GeV.

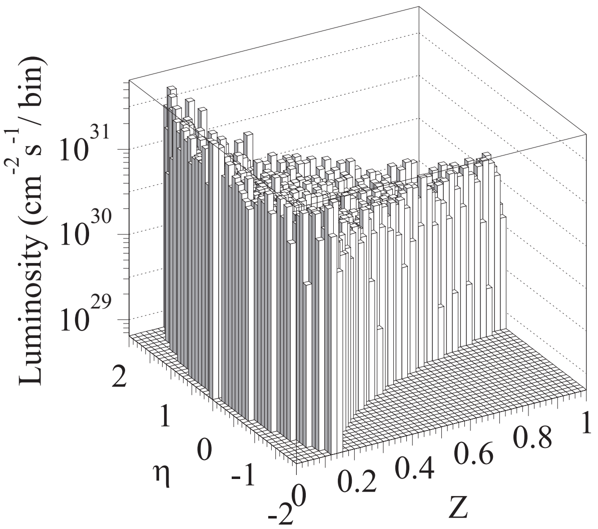

FIG. 15. The $\gamma\gamma$ luminosity distribution of a 5 TeV e^+e^- linear collider with $\Upsilon = 631$. The vertical axis is $d^2L_{\gamma\gamma}/dzd\eta$ in units of cm^{-2}s^{-1}/bin. The bin size $\Delta z \times \Delta\eta$ is 0.02×0.1.

---

[1] M. Bell and J.S. Bell, Part. Accel. **24**, 1 (1988); R. Blankenbecler and S.D. Drell, Phys. Rev. Lett. **61**, 2324 (1988); P. Chen and K. Yokoya, *ibid.* **61**, 1101 (1988); M. Jacob and T.T. Wu, Nucl. Phys. **B303**, 389 (1988); V.N. Baier, V.M. Katkov, and V.M. Strakhovenko, *ibid.* **B328**, 387 (1989); R. Blankenbecler and S.D. Drell, Phys. Rev. D **36**, 277 (1987); *ibid.* **37**, 3308 (1988); P. Chen, Phys. Rev. D **46**, 1186 (1992).

[2] T. Himel and J. Siegrist, in *Proceedings of the 2nd International Workshop on Laser Acceleration of Particles*, Los Angeles, CA, 7-18 Jan 1985.

[3] For an overall review, see K. Yokoya and P. Chen, in *Frontiers of Particle Beams: Intensity Limitations, Lecture Notes* in Physics Vol. 400 (Springer-Verlag, Berlin, 1992).

[4] International Linear Collider Technical Review Committee Report, SLAC-Report-471 (1995); Zeroth-Order Design Report for the Next Linear Collider, LBNL-PUB-5424, SLAC-Report-474 (1996); JLC Design Study, KEK-Report-97-1 (1997); Conceptual Design of a 500 GeV Electron Positron Linear Collider with Integrated X-Ray Laser Facility, DESY-97-048, ECFA-97-182 (1997).

[5] K. Yokoya, Nucl. Instrum. and Methods Phys. Res. A **251**, 1 (1986).

[6] A.A. Sokolov and I.M. Ternov, *Radiation from Relativistic Electrons*, AIP, Translation Series, New York, 1986.

[7] R.Noble, Nucl. Instrum. and Methods Phys. Res. A **256**, 427 (1987).

[8] *Proceedings of the 1996 DPF/DPB Summer Study on New Directions for High Energy Physics*, Snowmass, CO, 25 Jun - 12 Jul 1996.

[9] *Proceedings of the 7th Workshop on Advanced Accelerator Concepts*, Lake Tahoe, CA, 13-19 Oct 1996; *Proceedings of the 8th Workshop on Advanced Accelerator Concepts*, Baltimore, MD, 5-11 Jul 1998.

[10] M. Xie, T. Tajima, K. Yokoya, and S. Chattopadhyay, in *Proceedings of the 7th Workshop on Advanced Accelerator Concepts*, Lake Tahoe, CA, 13-19 Oct 1996; M. Xie, in *Proceedings of the 15th ICFA Advanced Beam Dynamics Workshop on Quantum Aspects of Beam Physics*, Monterey, CA, 4-9 Jan 1998; M. Xie, in *Proceedings of the 8th Workshop on Advanced Accelerator Concepts*, Baltimore, MD, 5-11 Jul 1998.

[11] P. Chen and K. Yokoya, Phys. Rev. D **38**, 987 (1988).

[12] P. Chen, T. Ohgaki, A. Spitkovsky, T. Takahashi, and K. Yokoya, Nucl. Instrum. and Methods Phys. Res. A **397**, 458 (1997).

[13] V.N. Baier and V.M. Katkov, Sov. Phys. JETP **26**, 854 (1968); W.Y. Tsai and T. Erber, Phys. Rev. D **10**, 492 (1974); P. Chen and V.I. Telnov, Phys. Rev. Lett. **63**, 1796 (1989).

[14] V.I. Ritus, Nucl. Phys. **B44**, 236 (1972).

[15] K.A. Thompson and P. Chen, in *Proceedings of the 8th Workshop on Advanced Accelerator Concepts*, Baltimore, MD, 5-11 Jul 1998.

[16] R. Engel and J. Ranft, Phys. Rev. D **54**, 4244 (1996).